Redox Biology 37 (2020) 101630

Contents lists available at ScienceDirect

Redox Biology

journal homepage: www.elsevier.com/locate/redox

Research Paper

Hysteresis and bistability in the succinate-CoQ reductase activity and reactive oxygen species production in the mitochondrial respiratory complex II

Nikolay I. Markevich [a,*], Miliausha H. Galimova [a], Lubov N. Markevich [b]

[a] Institute of Theoretical and Experimental Biophysics RAS, Pushchino, Moscow region, 142290, Russian Federation
[b] Institute of Cell Biophysics of RAS, Pushchino, Moscow region, 142290, Russian Federation

ARTICLE INFO

Keywords:
Complex II
Reactive oxygen species (ROS)
Computational model
Hysteresis
Bistability

ABSTRACT

The mitochondrial respiratory Complex II (CII) is one of key enzymes of cell energy metabolism, linking the tricarboxylic acid (TCA) cycle and the electron transport chain (ETC). CII reversibly oxidizes succinate to fumarate in the TCA cycle and transfers the electrons, produced by this reaction to the membrane quinone pool, providing ubiquinol QH_2 to ETC. CII is also known as a generator of reactive oxygen species (ROS).

It was shown experimentally that succinate can serve as not only a substrate in the forward succinate-quinone oxidoreductase (SQR) direction, but also an enzyme activator. Molecular and kinetic mechanisms of this property of CII are still unclear.

In order to account for activation of CII by succinate in the forward SQR direction, we developed and analyzed a computational mechanistic model of electron transfer and ROS formation in CII. It was found that re-binding of succinate to the unoccupied dicarboxylate binding site when FAD is reduced with subsequent oxidation of $FADH_2$ creates a positive feedback loop in the succinate oxidation. The model predicts that this positive feedback can result in hysteresis and bistable switches in SQR activity and ROS production in CII. This requires that the rate constant of re-binding of succinate has to be higher than the rate constant of the initial succinate binding to the active center when FAD is oxidized.

Hysteresis and bistability in the SQR activity and ROS production in CII can play an important physiological role. In the presence of hysteresis with two stable branches with high and low SQR activity, high SQR activity is maintained even with a very strong drop in the succinate concentration, which may be necessary in the process of cell functioning in stressful situations. For the same reason, a high stationary rate of ROS production in CII can be maintained at low succinate concentrations.

1. Introduction

The mitochondrial respiratory Complex II (CII) (succinate dehydrogenase (SDH) or succinate-coenzyme Q reductase (SQR)) is one of the most important enzymes of cell energy metabolism that serves as a link between the tricarboxylic acid (TCA) cycle and the electron transport chain (ETC). CII reversibly oxidizes succinate to fumarate, producing electrons that are transported via the Fe–S cluster chain to the ubiquinone membrane pool, thus providing QH_2 for the respiratory chain during oxidative phosphorylation. CII dysfunction can lead to either tumorigenesis or apoptosis depending on the physiological conditions [1,2]. In addition, mutation in SDH correlates with the onset of neurodegenerative disorders [3]. Therefore, CII can behave also as a key regulator in neuroprotection.

An important property of CII is the ability to generate reactive oxygen species (ROS) which play a crucial role not only in oxidative cellular damage and a development of various pathologies and aging but also function as critical mediators in a broad range of cellular signaling processes [4]. It was believed for a long time that within the respiratory chain complexes I and III (CI and CIII) were the main producers of ROS

Abbreviations: ROS, reactive oxygen species; CII, respiratory Complex II; ETC, electron transport chain; FAD, flavin adenine dinucleotide; SDH, succinate dehydrogenase; SQR, succinate CoQ oxidoreductase; SMP, submitochondrial particles.

* Corresponding author. Institute of Theoretical and Experimental Biophysics, Russian Academy of Sciences, 3 Institutskaya street, Pushchino, Moscow region, 14290, Russia.

E-mail address: markevich.nick@gmail.com (N.I. Markevich).

https://doi.org/10.1016/j.redox.2020.101630
Received 1 April 2020; Received in revised form 14 June 2020; Accepted 28 June 2020
Available online 5 July 2020

[5], although there were experimental data [6] allowing to conclude that CII can be a substantial source of ROS in mammalian mitochondria. It was found [6] that CII is the predominant generator of ROS during prolonged respiration under uncoupled conditions and CII appears to contribute to the basal production of ROS in cells. The most clear evidence of CII of mammalian mitochondria to be a significant source of ROS was demonstrated in studies of CII with the impairment of the succinate CoQ oxidoreductase (SQR) activity resulting from inhibition of CIII or Q-binding site of CII [7–9] as well as CII disintegration, i.e. the specific dissociation of the SDHA/SDHB subunits from the membrane-bound SDHC/SDHD complex that is required for the SQR activity [10]. Under these conditions CII could produce $O_2^{\cdot-}/H_2O_2$ in significant amounts, comparable and even exceeding ROS generated by CI and CIII, but only in the subsaturating range of the succinate concentration (50–500 μM).

It was shown experimentally more than three decades ago that CII has strong nonlinear properties in both, forward SQR and reverse quinol-fumarate reductase (QFR) directions [11–15]. For instance, succinate in the SQR direction can serve as not only a substrate, but also an enzyme activator [11]. Molecular and kinetic mechanisms of this property of CII are still unclear. One possible mechanism was proposed by Kotlyar and Vinogradov [11] who suggested that oxidation of succinate and FAD reduction results in an increase in the dissociation constant of the CII inhibitor oxaloacetate from the active center and thus removes the inhibitory effect of oxaloacetate. Although this explanation is applicable only to the kinetics of an activation of the oxaloacetate-inhibited succinate dehydrogenase. On the other hand, it was found in the voltammetry studies [12–14] as well as in the spectrophotometric kinetic assays with reduced benzylviologen as electron donor [15] that the soluble enzyme exhibits a “tunnel diode” behavior in the presence of fumarate, i.e., the rate of fumarate reduction decreases with increasing thermodynamic driving force. This means that the CII behavior resembles a tunnel diode, an electronic device exhibiting negative resistance [15,16].

In addition, it was found recently [17] that the excessive ROS production by CII under suppression of the activity of Complex III can result in autocatalytic mitochondrial permeability transition and activate death signaling pathways such as apoptosis or necrosis/necroptosis.

Despite of the important role of CII in the energy metabolism as well as in ROS production, unusual properties and mechanisms of ROS

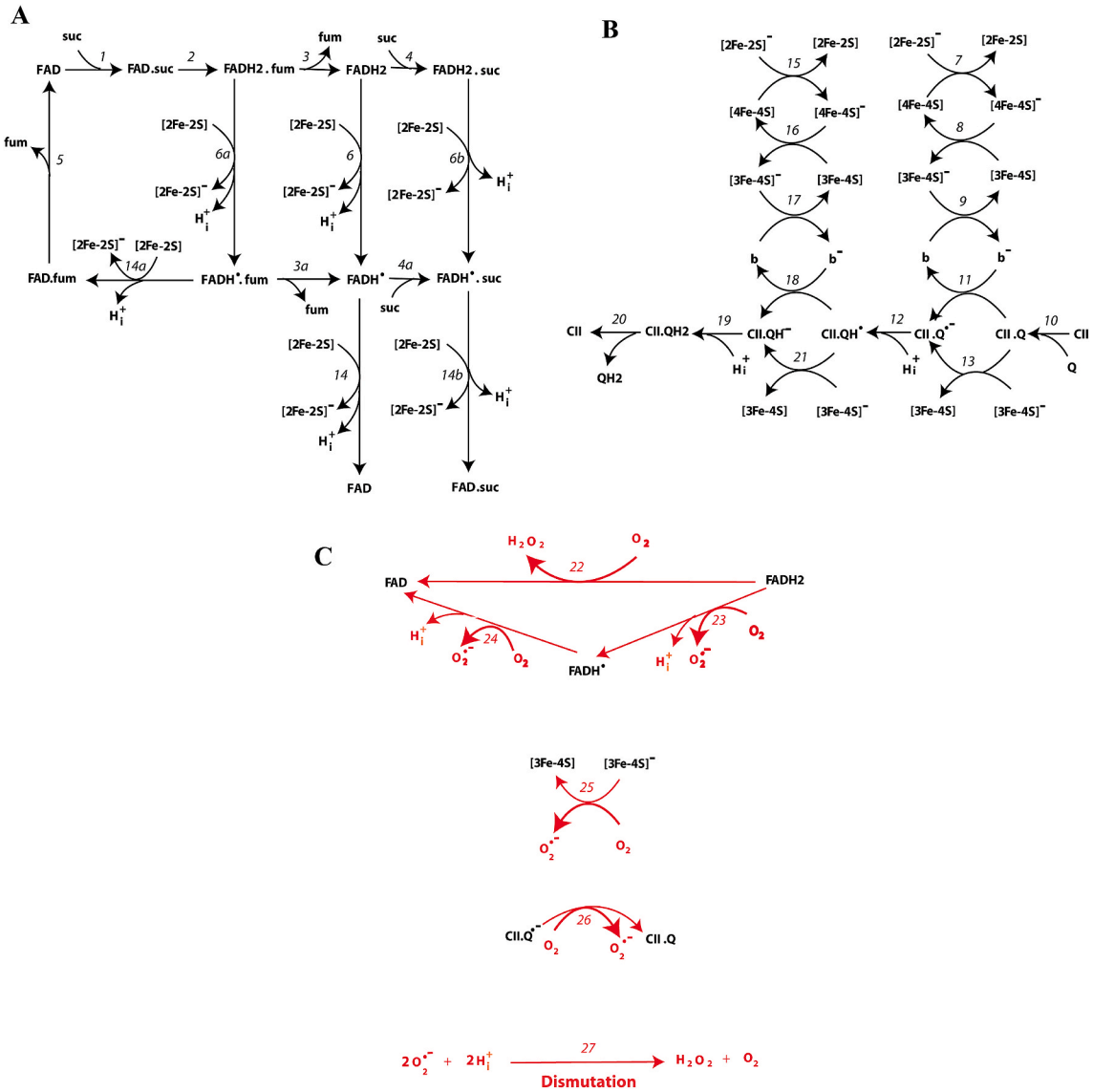

Fig. 1. Kinetic schemes of electron transfer and formation of superoxide anion, $O_2^{\cdot-}$, and hydrogen peroxide, H_2O_2, in the flavoprotein SDHA subunit (A) and subunits SDHB/SDHC/SDHD (B) of Complex II. Reactions of $O_2^{\cdot-}$ and H_2O_2 formation (C) are shown by red arrows. The detailed reaction network is presented in Supplementary Tables S1 and S2. (For interpretation of the references to colour in this figure legend, the reader is referred to the Web version of this article.)

formation by CII remain insufficiently understood. In order to answer some of these questions a computational mechanistic model of electron transfer and $O_2^{\cdot-}/H_2O_2$ formation at different redox centers of CII is developed in the present study which is a continuation of our previous theoretical studies of CII [18]. All the results in the current work relate only to the kinetic properties of CII in the forward SQR direction, that is, succinate oxidation and ubiquinone reduction. Computer analysis of the model reveals a hidden positive feedback loop and predicts that autocatalytic activation of the succinate oxidation reaction by succinate can lead to hysteresis and bistable switches in SQR activity as well as mitochondrial ROS production in CII when the succinate concentration changes.

It is important to point out that the mechanism for generating positive feedback and hysteresis behavior and bistability in CII is completely different from similar properties found earlier [19–21] in Complex III, which are the result of a feature of the Mitchell's Q-cycle kinetics.

2. Methods and models

A kinetic scheme of electron transfer and $O_2^{\cdot-}/H_2O_2$ production underlying a mechanistic computational model of CII is presented in Fig. 1. This scheme is supported by numerous literature data on succinate dehydrogenase (SDH) activity of CII, and electron transfer pathways between different redox centers of CII [7,9,11,22,23].

Fig. 1A presents chemical reactions of the reversible oxidoreductation of succinate, fumarate and FAD, catalyzed by the SDH flavoprotein subunit A (SDHA). These reactions involve a single electron transfer from reduced FAD to the first iron-sulfur, [2Fe–2S], cluster of the hydrophilic SDHB subunit. Reactions of electron transfer down the chain of iron-sulfur clusters towards the SDHC/SDHD subunits, and further down to quinone-binding site, where quinone Q is reduced to quinol QH_2, are shown in Fig. 1B. Reactions of the reactive oxygen species formation in CII are presented in Fig. 1C.

This kinetic scheme includes the following electron carriers: a) flavin adenine dinucleotide, FAD; b) the sequence of iron-sulfur clusters: [2Fe–2S], [4Fe–4S] and [3Fe–4S]; c) heme *b*; d) coenzyme Q. Electron transfer reactions in CII include both the mainstream electron pathway from succinate to coenzyme Q (SQR activity) and bypass reactions resulting in $O_2^{\cdot-}/H_2O_2$ formation. These bypass reactions are marked in red in the kinetic scheme (Fig. 1C). A brief description of kinetic schemes shown in Fig. 1A–C is given in Supplementary Data and individual chemical reactions are presented in Table S1.

The reaction network corresponding to the kinetic scheme depicted in Fig. 1 consists of 35 reactions, which are described by mass action and Michaelis-Menten (for superoxide anion dismutation) kinetics (Table S1). Midpoint redox potentials, rate constants and concentrations are taken from the experimental data (see Table S2 and references therein). The network dynamics is described by 20 ordinary differential equations (ODE) and 7 moiety conservation equations. Details of the mathematical model describing oxidized and reduced states of different carriers and electron flows through CII are presented in Supplementary Data. A model is implemented in DBSolve Optimum software available at http://insysbio.ru. Additionally, the model is presented in SBML format by separate file: markevich_CII model.xml (Supporting information).

3. Results and discussion

Analysis of quasi-stationary characteristics of the Complex II model. To find all stationary states it is convenient to analyze the so-called quasi-stationary concentration-response curves, which are calculated by assuming all concentrations except the concentration of FAD in the unoccupied dicarboxylate state to be at quasi-steady state (see Supplementary Data for details). Then, each Complex II (CII) steady state is determined when the total quasi-stationary rate of FAD production (V_{FAD_in}) becomes equal to the total quasi-stationary rate of FAD consumption (V_{FAD_out}). Using the kinetic schemes of Fig. 1, it can be readily seen that FAD is produced in reactions 5, 14 and 22, 24, that is, $V_{FAD\_in} = V_5 + V_{14} + V_{22} + V_{24} \sim V_5 + V_{14}$, whereas FAD is consumed only in reaction 1 when succinate binds to the dicarboxylate binding site of CII (see Supplementary Table S1). The points of intersection between these quasi-stationary curves give all possible steady states of CII (Fig. 2). This figure illustrates that there are three steady states, S_1, S_2 and S_3, at the same succinate concentration (120 μM). A reason for these tree points of intersection is a segment with the negative slope in the curve presenting the dependence of quasi-stationary rate V_{FAD_in} on FAD (Fig. 2B). In this segment, the FAD production rate V_{FAD_in} increases rather than decreases with FAD (product concentration), which is a feature of reactions with positive feedback. Two of the steady states, S_1 and S_3 are stable and one state, S_2, is unstable, meaning that even a minute initial deviation from S_2 will lead to a further departure toward states S_1 or S_3. An inherent feature of bistability is hysteresis, illustrated in Fig. 2A for the stationary dependence of the FAD concentration on the succinate concentration.

To better understand the properties of CII that result in a hidden positive feedback and the negative slope of the dependence of V_{FAD_in} on FAD, we vary the activity of different pathways involving the Flavin within a wide parameter range. We have change the rate constants k_6, k_{6a}, k_{6b} and k_{14}, k_{14a}, k_{14b} of electron transfer reactions by several orders of magnitude. Importantly, the negative slope in quasi-stationary concentration-response curves persist with wide parameter ranges (Fig. 3) and disappears only when reactions 6b and 14b of electron transfer from the complexes $FADH_2$.suc and $FADH^{\cdot}$.suc are blocked (Fig. 3C). Therefore, these electron transfer reactions play a key role, generating a positive feedback for the SDH reaction. This is easy to understand intuitively, because in reactions 6b and 14b the oxidation of $FADH_2$ and $FADH^{\cdot}$ occurs without releasing the succinate from the active center immediately to the FAD.suc state (Fig. 1A) and the repeated oxidation cycle of succinate is much facilitated since the initial step of binding of succinate to the active center in the reaction (1) is bypassed.

Hysteresis and bistability in the steady states of the CII model. Likewise, hysteresis is observed for the stationary rates of ubiquinone reductions (Fig. 4) and ROS production (Supplementary Fig. S1). The stationary total rate of H_2O_2 production by CII (vH_2O_2) was computed as the rate of H_2O_2 release from the mitochondrial matrix to cytosol that equal to the summary rate of H_2O_2 production by $FADH_2$, v_{22}, and dismutation of $O_2^{\cdot-}$, v_{27}, in the matrix at the steady state (see *Explicit functions* in Mathematical model in Supplementary Data).

The results illustrated in Fig. 4 and Supplementary Fig. S1 reiterate that hysteresis and bistability in the behavior of CII vanish if the electron transfer from the complexes of $FADH_2$ and $FADH^{\cdot}$ with succinate in the active center are inhibited (Fig. 4C and Supplementary Fig. S1C).

Additionally, Fig. 4D as well as Supplementary Fig. S1D illustrates how our finding of potential bistability in the stationary rates of ubiquinone reduction and ROS production by CII can be tested experimentally using a design similar to the one proposed earlier in the work on the prediction of bistability in protein kinase cascades [24]. Fig. 4D shows that adding or removing succinate leads to different stationary rates of ubiquinone reduction, v_{20}, at the same succinate concentration, depending on whether experimental manipulations have begun in the SQR activity "off" or "on" state that is a low or high stationary rate of ubiquinone reduction. If initially the SQR activity is in its off state, adding succinate causes a gradual increase in the rate of ubiquinone reduction, and only after the succinate concentration increases over a threshold, the SQR activity switches to its on state with a high rate of ubiquinone reduction (Fig. 4D, Going up). When starting with the on state of the SQR activity (Fig. 4D, Coming down), the succinate concentration can decrease to below the threshold, yet the stationary rate of ubiquinone reduction considerably exceeds this rate obtained for the same succinate concentration when beginning with the off state of the SQR activity. Similar arguments are valid for the hysteresis dependence of the stationary rate of ROS production on the succinate concentration

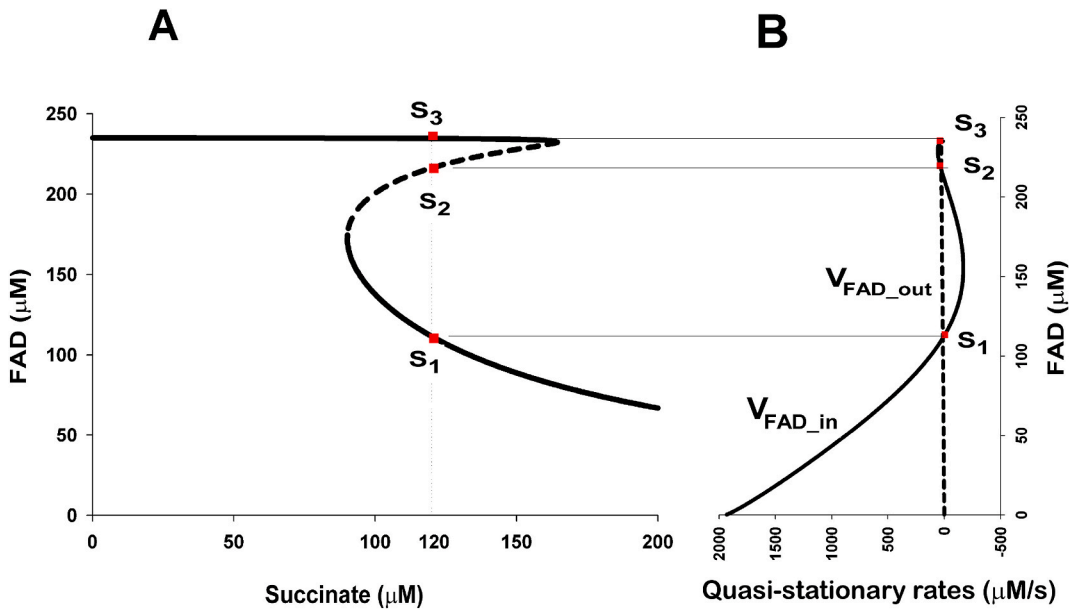

Fig. 2. Hysteresis and bistability in the respiratory Complex II. Three steady states, S1, S2, and S3 (panel A), correspond (panel B) to the three intersection points of the dependencies of quasi-stationary rates of FAD production V_{FAD_in} and consumption V_{FAD_out} on the FAD. concentration. The parameter values are as follows: (A, B) k1 = 10^{-3} $\mu M^{-1}s^{-1}$; (B) suc = 120 μM. The rest model parameters are presented in Supplementary Table S2.

shown in Supplementary Fig. S1D.

Parametric analysis of the appearance of hysteresis and bistability in the CII model. Computer analysis shows that the appearance of hysteresis and bistability in the CII model depends on many model parameters, one of the most important of which is the concentration of succinate. This directly follows from the results shown in Fig. 4 and Supplementary Fig. S1, which show that bistability in the stationary rates of ubiquinone reduction and ROS production, is observed only in a certain range of the succinate concentrations. Other most important parameters of the model are the rate constants k_1 and k_4, the first and second binding of succinate to the dicarboxylate binding site when FAD is oxidized or reduced, respectively. Detailed parametric analysis shows that the existence of hysteresis and bistability in the CII model strongly depends on the ratio of the rate constants k_1 and k_4 because these constants determine the effectiveness of the positive feedback in CII. According to computer calculations, hysteresis and bistability occur only when $k_4 > k_1$. More precisely, the critical values of the parameters k_1, k_4 and the succinate concentration at which hysteresis and bistability appear were calculated by computer analysis of saddle-node bifurcation in the mathematical model of CII, which in this case correspond to the transition from a single to three steady states, two stable and one unstable. By calculating critical parameter values at which the bifurcation appears, we obtain a bifurcation diagram that defines bistability domains. Supplementary Fig. S2 illustrates these domains in the plane of the succinate concentration and the rate constant k_1 (Fig. S2A), as well as of the rate constants k_4 and k_1 (Fig. S2B).

Bistability domains shown in Fig. S2A are calculated for different activities of three different electron pathway branches from $FADH_2$ in the unoccupied dicarboxylate state and complexes $FADH_2$.fum and $FADH_2$.suc to the first iron-sulfur cluster [2Fe–2S]. The bifurcation diagram in Fig. S2A confirms that bistable responses emerge even if $k_{6a} = k_{14a} = 0$, that is, when the electron transfer between $FADH_2$.fum and [2Fe–2S] is completely blocked (domain 2). At the same time, the bistability domain becomes much smaller compared to the bistability domain in the basal state (domain 1) when electron transfer between $FADH_2$.suc and [2Fe–2S] is at least partially blocked (domain 3), i.e. k_{6b} and k_{14b} decrease from 10^4 to 100 $\mu M^{-1}s^{-1}$, and the bistability domain disappears when k_{6b} and k_{14b} are reduced to 10 $\mu M^{-1}s^{-1}$.

Bistability domains in the plane of the rate constants k_1 and k_4 (Fig. S2B) are calculated for different succinate concentrations. A characteristic feature of these bistability domains is that k_1 is always less than k_4 and the k_1 values do not exceed 0.015 $\mu M^{-1}s^{-1}$. The fact that small values of k_1, that is, a low rate of the first binding of succinate to the dicarboxylate binding site when FAD is oxidized, are preferred for the appearance of hysteresis and bistability is readily to understand, since in this case it is easier to activate CII by faster the second binding of succinate the dicarboxylate binding site when FAD is reduced.

To illustrate the results obtained, the stationary rates of ROS generation by individual redox centers of CII at different values of the rate constant k_1 binding of succinate to the dicarboxylate binding site when FAD is oxidized are shown in Supplementary Fig. S3. From the results presented in Fig. S3, it can be seen that hysteresis and bistability in the rate of ROS generation by each considered redox center are observed in a wide range of succinate concentrations at small values of k_1 and disappear at $k_1 = 0.1$ $\mu M^{-1}s^{-1}$.

The computational mechanistic CII model under disease conditions. CII dysfunction resulting in different diseases is usually associated with changes in various SDH protein subunits: SDHA, SDHB, SDHC and SDHD. Changes can occur both at the level of their biogenesis and at the post-translational level (phosphorylation, acetylation, succinylation and so on) in response to multiple (patho)physiological stimulus. Different mechanisms have been proposed to explain the frequent clinical presentations associated with SDH dysfunction are discussed in review [2]. Mutations in any of subcomplexes should disrupt complex II enzymatic activity leading to various pathologies, for example, defects in SDHA produce bioenergetic deficiency while defects in SDHB, SDHC, or SDHD induce tumor formation [25]. In this study, the most interesting mutations in SDH are those that lead to an increase in the rate of ROS production by CII. This is first of all, defects in SDHB, SDHC and SDHD which correlate with paraganglioma, neuroendocrine neoplasm [26–28]. It is interesting to note that paragangliomas caused by SDHB mutations have several distinguishing characteristics, for example, malignancy is common in carriers with disease. In contrast, tumors caused by SDHD mutations are almost always benign [29]. This means that defects in SDHB and SDHD, in addition to the general property of increasing ROS generation by CII, have other specific effects on carcinogenesis. As already mentioned, an impairment of the transfer of electrons from $FADH_2$ to ubiquinone, i.e., impairment SQR activity,

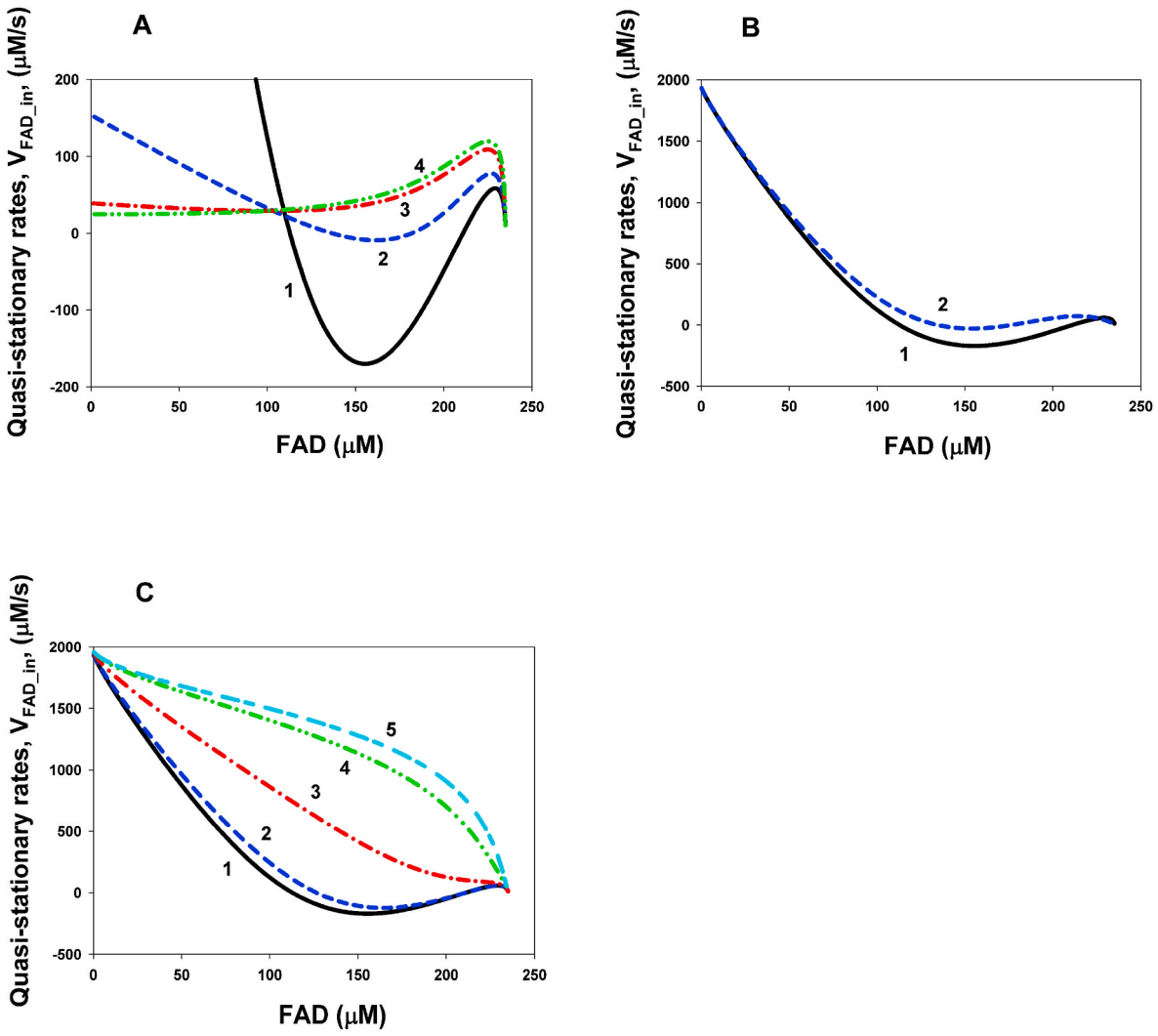

Fig. 3. Effects of the activity of electron transfer between reduced FAD and [2Fe–2S] cluster on the dependence of the quasistationary rate V_{FAD_in} on the concentration of oxidized FAD in Complex II for three different electron pathway branches. (A) Electron pathway from $FADH_2$ in the unoccupied dicarboxylate state. Black solid curve (1) corresponds to $k_6 = k_{14} = 10^4$ $\mu M^{-1}s^{-1}$, blue dashed curve (2) – $k_6 = k_{14} = 10$ $\mu M^{-1}s^{-1}$, red dash-dot curve (3) – $k_6 = k_{14} = 1$ $\mu M^{-1}s^{-1}$, green dash-dot-dot curve (4) – $k_6 = k_{14} = 0$. (B) Electron pathway from complex $FADH_2$.fum to [2Fe–2S] cluster. Black solid curve (1) corresponds to $k_{6a} = k_{14a} = 10^4$ $\mu M^{-1}s^{-1}$, blue dashed curve (2) – $k_{6a} = k_{14a} = 0$. (C) Electron pathway from the complex $FADH_2$.suc to [2Fe–2S] cluster. Black solid curve (1) corresponds to $k_{6b} = k_{14b} = 10^4$ $\mu M^{-1}s^{-1}$, blue dashed curve (2) – $k_{6b} = k_{14b} = 10^3$ $\mu M^{-1}s^{-1}$, red dash-dot curve (3) – $k_{6b} = k_{14b} = 10^2$ $\mu M^{-1}s^{-1}$, green dash-dot-dot curve (4) – $k_{6b} = k_{14b} = 10$ $\mu M^{-1}s^{-1}$, cyan short-long curve (5) – $k_{6b} = k_{14b} = 1$ $\mu M^{-1}s^{-1}$. $k_1 = 10^{-3}$ $\mu M^{-1}s^{-1}$, suc = 120 μM, fum = 0. The rest model parameters are presented in Supplementary Table S2. . (For interpretation of the references to colour in this figure legend, the reader is referred to the Web version of this article.)

leads to a strong increase in ROS generation, which is assumed [7,8] to be associated with an increase in the concentration of reduced FAD. According to the model, a strong decrease in the electron transfer rates from $FADH_2$ and $FADH^{\cdot}$ to the SDHB subunit iron clusters [2Fe–2S] (v_6, v_{6a}, v_{6b} and v_{14}, v_{14a}, v_{14b}) can be due to a decrease in the rate constants k_6, k_{6a}, k_{6b} and k_{14}, k_{14a}, k_{14b} with defects in SDHB. Another though less likely reason may be a decrease in the electron transfer rate constants within the SDHB subcomplex between different Fe–S centers. With defects in SDHC and SDHD, this can be an impairment the Q-binding site and inhibition of electron transfer from the cluster [3Fe–4S] and heme *b* to ubiquinone, which also leads to a strong reduction of potential redox centers of ROS formation, $FADH_2$ and cluster [3Fe–4S], and an increase in the rate of ROS formation by these redox centers. In particular, it was found that a point mutation at the ubiquinone binding region in the SDHC gene increased $O_2^{\cdot-}$ production from CII [28]. One possible way to inhibit SQR activity with defects in SDHC and SDHD is to inhibit the binding of the oxidized Q to the Q-binding site, that is, to reduce the rate v_{10} in our mechanistic model. Supplementary Fig. S4 shows dependences of the stationary rates of QH_2 production and ROS formation by different sites of CII when the binding constant k_{10} is reduced from 10 to 0.002 $\mu M^{-1}sec^{-1}$. The results of computer simulation of inhibition of the Q-binding site show that the hysteresis in the stationary rates of both Q reduction, v_{20} (Fig. S4A), and ROS generation (Figs. S4B–F) persist with wide k_1 ranges. First of all, it is easy to understand that the maximum steady-state rate of ubiquinone reduction, v_{20}, drops significantly when k_{10} decreases from 10 to 0.002 $\mu M^{-1}s^{-1}$ (compare Fig. 4 in the main text and Supplementary Fig. S4A). At the same time, the rate of formation of superoxide by semiquinone, v_{26}, also decreases (compare Fig. S3E and Fig. S4), but the rate of generation of $O_2^{\cdot-}$ by $FADH_2$, v_{23}, at k10 = 0.002 $\mu M^{-1}s^{-1}$ (Fig. S4C) increases almost 5 times compared to the rate in the basal state when $k_{10} = 10$ $\mu M^{-1}s^{-1}$ (Fig. S3B). Thus, the total rate of ROS generation by CII increases under inhibition of the Q-binding site (Fig. S4B) compare to the basal state (Fig. S3F).

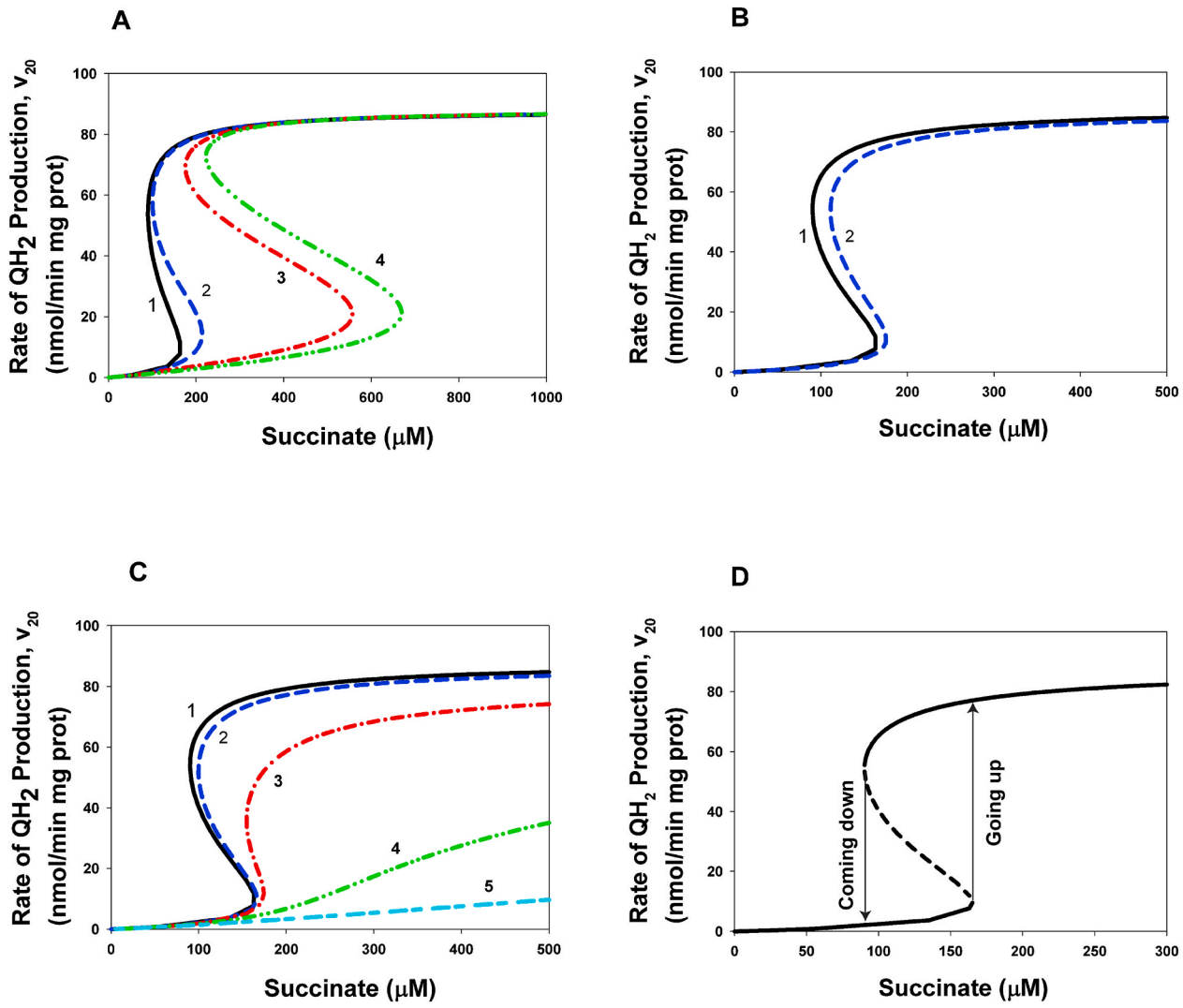

Fig. 4. Effects of the activity of electron transfer between reduced FAD and [2Fe–2S] cluster on the dependence of the stationary rate of ubiquinone reduction, V_{20}, on the succinate concentration in Complex II for three different pathway branches. (A) Electron pathway from $FADH_2$ in the unoccupied dicarboxylate state. Black solid curve (1) corresponds to $k_6 = k_{14} = 10^4$ $\mu M^{-1}s^{-1}$, blue dashed curve (2) – $k_6 = k_{14} = 10$ $\mu M^{-1}s^{-1}$, red dash-dot curve (3) – $k_6 = k_{14} = 1$ $\mu M^{-1}s^{-1}$, green dash-dot-dot curve (4) – $k_6 = k_{14} = 0$. **(B)** Electron pathway from $FADH_2$ in the occupied dicarboxylate state by fumarate. Black solid curve (1) corresponds to $k_{6a} = k_{14a} = 10^4$ $\mu M^{-1}s^{-1}$, blue dashed curve (2) – $k_{6a} = k_{14a} = 0$. (**C**) Electron pathway from $FADH_2$ in the occupied dicarboxylate state by succinate. Black solid curve (1) corresponds to $k_{6b} = k_{14b} = 10^4$ $\mu M^{-1}s^{-1}$, blue dashed curve (2) – $k_{6b} = k_{14b} = 10^3$ $\mu M^{-1}s^{-1}$, red dash-dot curve (3) – $k_{6b} = k_{14b} = 10^2$ $\mu M^{-1}s^{-1}$, green dash-dot-dot curve (4) – $k_{6b} = k_{14b} = 10$ $\mu M^{-1}s^{-1}$, cyan short-long curve (5) – $k_{6b} = k_{14b} = 1$ $\mu M^{-1}s^{-1}$. (**D**) The curve shown in this figure corresponds to curves (1) in Figs A–C only on a scale 0–300 μM of the succinate concentration. Model parameters are presented in Supplementary Table S2 except $k_1 = 10^{-3}$ $\mu M^{-1}s^{-1}$, fum = 0. . (For interpretation of the references to colour in this figure legend, the reader is referred to the Web version of this article.)

4. Conclusion

A computational mechanistic model of electron transfer and formation of superoxide ($O_2^{\cdot-}$) and hydrogen peroxide (H_2O_2) in the respiratory Complex II (CII) of the inner mitochondrial membrane was developed to facilitate the quantitative analysis of the kinetics of succinate-coenzyme Q oxidoreductation (SQR) as well as mitochondrial reactive oxygen species (ROS) production and to assist in the interpretation of experimental studies. The model consists of 20 ordinary differential equations and 7 moiety conservation equations that describe the concentration of oxidized and reduced states of different redox centers and electron flows in CII.

Computer analysis of the model predicts positive feedback and autocatalytic activation of the succinate oxidation reaction by succinate, which lead to hysteresis and bistable switches in SQR activity as well as mitochondrial ROS production in CII when the succinate concentration changes. A key reason for the appearance of autocatalytic properties in CII in the forward electron transfer direction from succinate to ubiquinone in the Q-binding site is the second binding of succinate to the dicarboxylate binding site after FAD is reduced to $FADH_2$. In this case, the oxidation of $FADH_2$ to FAD after the transfer of two electrons to the [2Fe–2S] cluster occurs without releasing the succinate from the active center and the subsequent oxidation of the second succinate molecule is greatly facilitated, since the succinate is already in the active center and its initial binding is not required.

Detailed parametric analysis shows that the existence of hysteresis and bistability in the Complex II model strongly depends on the ratio of the rate constants k_1 (the initial succinate binding to the active center when FAD is oxidized) and k_4 (the second binding of succinate to the active center when FAD is reduced to $FADH_2$) because these constants determine the effectiveness of the positive feedback in Complex II. According to computer calculations, hysteresis and bistability occur only when $k_4 > k_1$, that is the rate constant of re-binding of succinate has to be higher than the rate constant of the initial succinate binding to the

active center. More precisely, the critical values of the parameters k_1 and k_4 as well as the succinate concentration at which hysteresis and bistability appear, bistability domains, were calculated by computer analysis of saddle-node bifurcation in the mathematical model of Complex II.

The real values of the rate constants k_1 and k_4 are unknown, so our current results are purely predictive hypothesis. So, experimental confirmation of our predictions of hysteresis and bistability in the kinetics of succinate oxidation by Complex II is needed. These effects will be observed in cells with a strong positive feedback, that is, in cells in which k_1 is less than k_4.

Computer simulation of a decrease in the rate constant of Q binding to the Q-binding site, k_{10}, that can result from defects in SDHC or SDHD subcomplexes of CII under different diseases shows that hysteresis and bistability in the stationary rates of both Q reduction and ROS generation persist with wide k_1 ranges. In addition, inhibition of the Q-binding site leads to a strong increase in the maximum stationary rate of ROS production at the flavin site, while a decrease in the production of superoxide by semiquinone at the Q-binding site. At the same time, the total rate of ROS generation by CII increases.

Hysteresis and bistability in the stationary dependence of the rate of succinate oxidation and ubiquinone reduction on the succinate concentration can play an important physiological role. In the presence of a hysteresis with two stable branches with high and low SQR activity, high SQR activity persists even with a very strong drop in the concentration of succinate in the mitochondria, which may be necessary in the course of cell functioning in stressful situations. For the same reason, if necessary, the high stationary rate of ROS production in complex II can be maintained at low succinate concentrations.

Author contributions

N.I.M. conceived and supervised the study; M.H.G., L.N.M. and N.I.M. performed computations; N.I.M. and M.H.G. wrote this report.

Formatting of funding sources

This research did not receive any specific grant from funding agencies in the public, commercial, or not-for-profit sectors. The work was carried out with budget funding under the State assignment of the Institute of Theoretical and Experimental Biophysics of the Russian Academy of Sciences (ITEB RAS) No. 075-00845-20-01. We are grateful to Administration of ITEB RAS for covering open access publication fee.

Declaration of competing interest

No conflicts of interest, financial or otherwise, are declared by the authors.

Acknowledgements

We thank Prof. Boris N. Kholodenko for critical reading of this manuscript and numerous useful tips and comments.

Appendix A. Supplementary data

Supplementary data to this article can be found online at https://doi.org/10.1016/j.redox.2020.101630.

References

[1] S. Grimm, Respiratory chain complex II as general sensor for apoptosis, Biochim. Biophys. Acta 1827 (5) (2013) 565–572, https://doi.org/10.1016/j.bbabio.2012.09.009.

[2] A. Bezawork-Geleta, J. Rohlena, L. Dong, K. Pacak, J. Neuzil, Mitochondrial complex II: at the crossroads, Trends Biochem. Sci. 42 (4) (2017) 312–325, https://doi.org/10.1016/j.tibs.2017.01.003.

[3] M. Jodeiri Farshbaf, A. Kiani-Esfahani, Succinate dehydrogenase: prospect for neurodegenerative diseases, Mitochondrion 42 (2018) 77–83, https://doi.org/10.1016/j.mito.2017.12.002.

[4] M. Ristow, K. Schmeisser, Mitohormesis: promoting health and lifespan by increased levels of reactive oxygen species (ROS), Dose Response 12 (2014) 288–341, https://doi.org/10.2203/dose-response.13-035.

[5] S. Dröse, U. Brandt, Molecular mechanisms of superoxide production by the mitochondrial respiratory chain, Adv. Exp. Med. Biol. 748 (2012) 145–169, https://doi.org/10.1007/978-1-4614-3573-0_6.

[6] H.R. McLennan, M. Degli Esposti, The contribution of mitochondrial respiratory complexes to the production of reactive oxygen species, J. Bioenerg. Biomembr. 32 (2000) 153–162, https://doi.org/10.1023/a:1005507913372.

[7] C.L. Quinlan, A.L. Orr, I.V. Perevoshchikova, J.R. Treberg, B.A. Ackrell, M. D. Brand, Mitochondrial complex II can generate reactive oxygen species at high rates in both the forward and reverse reaction, J. Biol. Chem. 287 (2012) 27255–27264, https://doi.org/10.1074/jbc.M112.374629.

[8] I. Siebels, S. Dröse, Q-site inhibitor induced ROS production of mitochondrial complex II is attenuated by TCA cycle dicarboxylates, Biochim. Biophys. Acta 1827 (2013) 1156–1164, https://doi.org/10.1016/j.bbabio.2013.06.005.

[9] V.G. Grivennikova, V.S. Kozlovsky, A.D. Vinogradov, Respiratory complex II: ROS production and the kinetics of ubiquinone reduction, Biochim. Biophys. Acta 1858 (2017) 109–117, https://doi.org/10.1016/j.bbabio.2016.10.008.

[10] M.-S. Hwang, J. Rohlena, L.-F. Dong, J. Neuzil, S. Grimm, Powerhouse down: complex II dissociation in the respiratory chain, Mitochondrion 19 (2014) 20–28, https://doi.org/10.1016/j.mito.2014.06.001.

[11] A.B. Kotlyar, A.D. Vinogradov, Interaction of the membrane-bound succinate dehydrogenase with substrate and competitive inhibitors, Biochim. Biophys. Acta 784 (1) (1984) 24–34, https://doi.org/10.1016/0167-4838(84)90168-7.

[12] Sucheta, B.A. Ackrell, B. Cochran, F.A. Armstrong, Diode-like behaviour of a mitochondrial electron-transport enzyme, Nature 356 (6367) (1992) 361–362, https://doi.org/10.1038/356361a0.

[13] J. Hirst, A. Sucheta, B.A. Ackrell, F.A. Armstrong, Electrocatalytic voltammetry of succinate dehydrogenase: direct quantification of the catalytic properties of a complex electron-transport enzyme, J. Am. Chem. Soc. 118 (1996) 5031–5038.

[14] H.R. Pershad, J. Hirst, B. Cochran, B.A. Ackrell, F.A. Armstrong, Voltammetric studies of bidirectional catalytic electron transport in Escherichia coli succinate dehydrogenase: comparison with the enzyme from beef heart mitochondria, Biochim. Biophys. Acta 1412 (1999) 262–272, https://doi.org/10.1016/s0005-2728(99)00066-3.

[15] B.A. Ackrell, F.A. Armstrong, B. Cochran, A. Sucheta, T. Yu, Classification of fumarate reductases and succinate dehydrogenases based upon their contrasting behavior in the reduced benzylviologen/fumarate assay, FEBS Lett. 326 (1–3) (1993) 92–94, https://doi.org/10.1016/0014-5793(93)81768-u.

[16] V.W. Cheng, R.S. Piragasam, R.A. Rothery, E. Maklashina, G. Cecchini, Redox state of flavin adenine dinucleotide drives substrate binding and product release in Escherichia coli succinate dehydrogenase, Biochemistry 54 (4) (2015) 1043–1052, https://doi.org/10.1021/bi501350j.

[17] P. Korge, S.A. John, G. Calmettes, J.N. Weiss, Reactive oxygen species production induced by pore opening in cardiac mitochondria: the role of complex II, J. Biol. Chem. 292 (24) (2017) 9896–9905, https://doi.org/10.1074/jbc.M116.768325.

[18] N.I. Markevich, M.H. Galimova, L.N. Markevich, Mathematical model of electron transfer and formation of reactive oxygen species in mitochondrial complex II, Biochem. Moscow Suppl. Ser. A 13 (2019) 341–351, https://doi.org/10.1134/S199074781904007X.

[19] V.A. Selivanov, T.V. Votyakova, J.A. Zeak, M. Trucco, J. Roca, M. Cascante, V. 5. P. e1000619, PLoS Comput. Biol. (2009), https://doi.org/10.1371/journal.pcbi.100061.

[20] J.N. Bazil, K.C. Vinnakota, F. Wu, D.A. Beard, Analysis of the kinetics and bistability of ubiquinol:cytochrome c oxidoreductase, Biophys. J. 105 (2013) 343–355, https://doi.org/10.1016/j.bpj.2013.05.033.

[21] N.I. Markevich, J.B. Hoek, Computational analysis of hysteresis and bistability in the mitochondrial respiratory chain, Math. Biol. Bioinformatics 9 (2014) 89–111.

[22] E. Maklashina, G. Cecchini, S.A. Dikanov, Defining a direction: electron transfer and catalysis in Escherichia coli complex II enzymes, Biochim. Biophys. Acta 1827 (5) (2013) 668–678, https://doi.org/10.1016/j.bbabio.2013.01.010.

[23] R.F. Anderson, S.S. Shinde, R. Hille, R.A. Rothery, J.H. Weiner, S. Rajagukguk, E. Maklashina, G. Cecchini, Electron transfer pathways in the heme and quinine-binding domain of Complex II, Biochemistry 53 (10) (2014) 1637–1646, https://doi.org/10.1021/bi401630m.

[24] N.I. Markevich, J.B. Hoek, B.N. Kholodenko, Signaling switches and bistability arising from phosphorylation in protein kinase cascades, J. Cell Biol. 164 (2004) 353–359, https://doi.org/10.1083/jcb.200308060.

[25] R.D. Guzy, B. Sharma, E. Bell, N.S. Chandel, P.T. Schumacker, Loss of the SdhB, but Not the SdhA, subunit of complex II triggers reactive oxygen species-dependent hypoxia-inducible factor activation and tumorigenesis, Mol. Cell Biol. 28 (2008) 718–731, https://doi.org/10.1128/MCB.01338-07.

[26] S. Niemann, U. Muller, Mutations in SDHC cause autosomal dominant paraganglioma, type 3, Nat. Genet. 26 (2000) 268–270, https://doi.org/10.1038/81551.

[27] B.E. Baysal, R.E. Ferrell, J.E. Willett-Brozick, E.C. Lawrence, D. Myssiorek, A. Bosch, A. van der Mey, P.E. Taschner, W.S. Rubinstein, E.N. Myers, C.W. r. Richard, C.J. Cornelisse, P. Devilee, B. Devlin, Mutations in SDHD, a

mitochondrial complex II gene, in hereditary paraganglioma, Science 287 (2000) 848–851, https://doi.org/10.1126/science.287.5454.848.

[28] T. Ishii, K. Yasuda, A. Akatsuka, O. Hino, P.S. Hartman, N. Ishii, A mutation in the SDHC gene of complex II increases oxidative stress, resulting in apoptosis and tumorigenesis, Canc. Res. 65 (2005) 203–209. PMID: 15665296.

[29] H.P. Neumann, C. Pawlu, M. Peczkowska, B. Bausch, S.R. McWhinney, M. Muresan, M. Buchta, G. Franke, J. Klisch, T.A. Bley, S. Hoegerle, C.C. Boedeker, G. Opocher, J. Schipper, A. Januszewicz, C. Eng, Distinct clinical features of paraganglioma syndromes associated with SDHB and SDHD gene mutations, J. Am. Med. Assoc. 292 (2004) 943–951, https://doi.org/10.1001/jama.292.8.943.